# Analysis, Design and Performance Evaluation of On-Chip Optical Wireless Links

Jinous Shafiei Dehkordi
Velio Tralli

Engineering Department
University of Ferrara
Ferrara, Italy
Email: shfjns@unife.it
velio.tralli@unife.it

Marina Barbiroli
Jacopo Nanni
Franco Fuschini

DEI - University of Bologna, Italy
Email: marina.barbiroli@unibo.it
jacopo.nanni3@unibo.it
franco.fuschini@unibo.it

Vincenzo Petruzzelli

Polytechnic of Bari
Bari, Italy
Email: vincenzo.petruzzelli
@poliba.it

***Abstract*—In Network-on-Chips (NoCs), Optical Wireless (OW) interconnects have recently gained attention to overcome the limitations of existing wired and wireless Radio Frequency (RF) technologies, while preserving the bandwidth and delay characteristics of optical interconnects. In this paper, we investigate the communication performance of the on-chip OW links by considering the effects of both wireless propagation and inter-link interference, which arises when the same optical frequency is used for multiple transmissions in a NoC. A Ray Tracing (RT) approach is applied to the layered structure of the on-chip wireless channel to obtain accurate modeling of multipath propagation. By using the Ray Tracing (RT) results, the Bit Error Probability (BEP) is evaluated as a function of desired and interfering signal powers, which depend on the far-field spatial fading conditions. The physical parameters and the geometry of the scenario, and the impact of antenna radiation pattern are taken into account in the evaluation. The analysis and the results enable system designers to design and provide efficient on-chip interconnects, optimizing not only the topology of the OW links in the NoC, but also the physical parameters of the links, including antenna characteristics, that influence the wireless communication.**

***Keywords*—*Optical wireless links; On-chip communications; Performance evaluation; Ray tracing.***

## I. INTRODUCTION

Optical Wireless (OW) links have recently emerged as an interconnection technology for Network-on-Chips (NoCs) [1] [2]. The NoC technology [3] requires highly reliable communications among multiple processing cores, whereas interconnecting on-chip components is a long-standing problem [4][5]. The continuously growing need for low-power and high-speed communication asks for efficient on-chip interconnects. The number of nodes in NoCs is predicted to increase significantly in the near future. In such networks, the traditional scaling of metal interconnections cannot satisfy the communication requirements due to their limitations in power consumption and bandwidth. To overcome these problems, alternative approaches like optical interconnections using silicon photonics [6][7] and wireless interconnections using Radio Frequency (RF) technologies [8]–[11], were considered.

Optical NoCs exploit optical frequency to provide high data rate communication, while reducing propagation losses and delays [6][7]. However, as the number of on-chip cores increases, the realization of optical NoCs with wired architecture becomes very complicated, which is followed by increasing complexity of switching and routing, and power losses due to multiple waveguide crossings. Providing point-to-point communication between cores and the limitations of wired architectures to support multi-cast and broadcast transmissions are the main challenges of such networks.

Wireless communication has gained a wide interest for multicore system-on-chip as an efficient solution to replace long distance on-chip interconnects [9][10], thus simplifying routing and layout complexity. Wireless on-chip communications also reduce latency and power consumption, and improve broadcast communications in large-scale chip multiprocessors [12]. However, RF wireless communications cannot provide the same bandwidth as optical technology, and present significant challenges for on-chip antenna integration [13].

OW interconnects can take advantages of both the optical and wireless communication [1][2]. This on-chip interconnect technology exploits broadcast and multicast transmissions at optical frequencies with simple network architectures and efficient use of the chip area. The OW links can be realized by coupling optical nanoantennas with optical waveguides, where the same wavelength propagating on optical waveguides can be used for wireless connections. Therefore, there is no need for any electro-optical conversion and increasing power consumption, and latency. Nevertheless, there are several challenges for using OW links in NoCs that must be addressed accurately. The OW links operating on the same wireless channel (optical wavelength) may interfere with each other, which degrades communication performance [14].

We aim to study the effects of both wireless propagation and interference on the communication performance in NoCs using OW links. The antenna radiation pattern, the geometry of the scenario and the various parameters characterizing the layered structure of the chip are considered. In particular, propagation channel is characterized by using a RT method, which tracks multipath fading in the on-chip wireless channel [15]. The Bit Error Probability (BEP) is evaluated as a function of desired

 ISBN: 978-1-61208-749-8

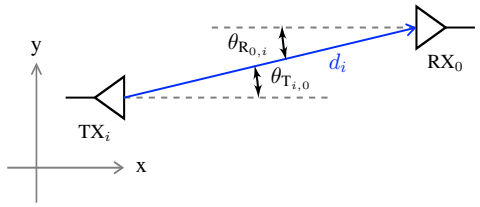


Figure 1. Top view of a OW link.

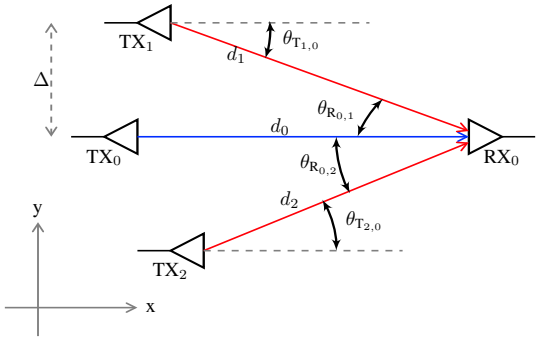


Figure 2. Top view of multiple OW links.

and interfering signal powers, which are subject to far-field spatial fading. The results allow a system designer to find the optimal OW links configuration in the NoC, such that a specified BEP is satisfied for the on-chip communications.

The remainder of this paper is organized as follows. Section II presents the scenario of the NoC. In Section III, the propagation channel is modeled in the layered structure of the chip. Section IV describes the system model and evaluates the BEP considering both interference and noise in the NoC. Section V provides some numerical results for different network configurations. Finally, Section VI gives our conclusions.

## II. On-chip communication scenario

Consider a NoC, where nodes are communicating through OW links. For each link, the source of the optical power is an external off-chip laser coupled to an optical bus or waveguide. Then, a Micro Ring Resonator (MRR) carries out both electrical-to-optical conversion and digital modulation of the optical carrier. Finally, the modulated signal is radiated within the chip through the optical antenna. At the receiving end of the wireless link, the optical impinging signal is seized by the optical receiving antenna, filtered by a second MRR and converted by a photodiode into the electrical domain.

The frequency reuse concept is used to improve spectrum efficiency. By reusing the same optical wavelength in multiple links, the number of simultaneous communications will not be limited by the number of available wavelengths. In particular, we consider the general case where there are $N+1$ wireless links that use the same frequency and may interfere with each other. Figure 1 shows the top view of the wireless part of a single link, where the antenna of the probe receiver RX$_0$ receives the optical signal from the antenna of the $i$-th transmitter TX$_i$. The distance between the antennas is $d_i$. In the figure, dashed lines show the antenna axes, $\theta_{T_{i,0}}$ is the angle between the transmitting direction and TX$_i$ antenna axis, and $\theta_{R_{0,i}}$ is the angle between the receiving direction and RX$_0$ antenna axis. Figure 2 shows a scenario with multiple links, where the desired link is interfered by the adjacent links, i.e., TX$_1$ and TX$_2$. We use index $i=0$ (TX$_0$) for the transmitting side of the desired link, and indexes $i=1,2,\ldots,N$ for the interfering links. We assume that the transmit antenna of TX$_0$ is located at the position $(x_{\text{TX}_0}, y_{\text{TX}_0}) = (0,0)$ in the horizontal plane. The receive antenna of RX$_0$ is located at distance $d_0 = (x_{\text{RX}_0}^2 + y_{\text{RX}_0}^2)^{1/2}$ from TX$_0$, and is rotated versus the TX$_0$ antenna. Thus, the maximum gain for transmitting and receiving antennas in the desired link is achieved.

As long as a single link is considered, communication errors are mainly due to the propagation conditions and to the noise effect that influence the optical system. In contrast, if a multi-link scenario is addressed, mutual interference can arise between the simultaneous links, to an extent that depends on antenna radiation patterns and reciprocal positions of the interfering links.

## III. Channel modeling

We use a 3D RT to characterize the far-field spatial fading of the on-chip wireless channel [15]. In particular, we refer to the optical frequency of 193.5 THz, corresponding to wavelength $\lambda = 1.55\,\mu m$ in vacuum. The layered structure of the chip and the electromagnetic properties of the materials are also considered in the analysis. Figure 3 shows the side view (in xz plane) of each OW link in Figure 1. The transmit and receive antennas are placed at the middle of a homogenous $SiO_2$ layer with the thickness $h_{\text{slb}}$ in the range of (4-10) $\mu m$. The thickness of the up and down layers are denoted by $h_{\text{up}}$ and $h_{\text{down}}$, respectively. Wave propagation occurs within the $SiO_2$ slab, which experiences reflections from the interfaces with surrounding mediums, thus causing multipath effects [1] [2][15]–[17]. The upper medium above the $SiO_2$ layer can be air or a different passivation material, the down layer can be silicon or metal. By considering the chip layered structure, multipath is fundamentally generated by multiple reflections between the interfaces of different media (see Figure 3), which can be evaluated by using the RT approach as in [1][15]. Note that the RT modeling is particularly employed for the investigation of the optical wireless channel, as geometrical optic is expected to become more reliable as frequency increases.

In the RT simulations, both geometrical and electromagnetic properties of the wireless links have to be taken into account. The geometrical parameters include the $SiO_2$ layer thickness ($h_{\text{slb}}$ in Figure 3), the antenna distance from the interfaces ($z=0$ is at the middle of the $SiO_2$ layer with the same distances from the upper and lower interfaces) and the wireless link length (i.e., distance between transmitting and receiving antennas). The electromagnetic parameters include the material refraction index of each layer of the chip ($n_{\text{down}}$, $n_{\text{slb}}$ and

 ISBN: 978-1-61208-749-8 

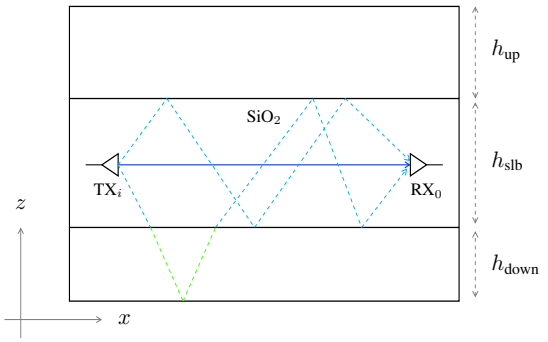


Figure 3. Side view of chip layered structure.

$n_{up}$). A 3D representation of the antenna radiation patterns is also necessary for RT modeling. The assessment carried out in this work is based on an idealized model for the antenna radiation diagram, but any other antenna configurations can be embedded into the RT tool. In particular, the gain of the antenna in a given direction is determined by the following expression.

$$g(\alpha,\phi) = \begin{cases} 10\log_{10}(G\cos(\phi)^n \cos(\pi/2-\alpha)^n) & \text{if } |\phi| < \frac{\pi}{2} \\ -50\,\text{dB} & \text{otherwise} \end{cases} \quad (1)$$

where $n = (10^{0.1\,G_{\text{dB}})})/2 - 1$, $G$ is the antenna gain, $\alpha$ is the elevation angle and $\phi$ the azimuth angle. Although rays in Figure 3 lie in the vertical ($xz$) plane, the 3D representation of the antenna radiation pattern is necessary, in order for the RT simulation to be run irrespective of the antenna orientation with respect to the propagation plane, e.g., to estimate the power arriving from an interfering transmitter. Once the rays have been tracked and the fields impinging on the receiver have been computed, the overall received power can be evaluated as illustrated in [15]. The important parameters considered for the RT simulations are summarized in Table I.

TABLE I. RT PARAMETERS.

| RT simulation parameters | |
|---|---|
| $h_{up}$ | $\infty$ |
| $h_{slb}$ | 4-10 $\mu$m |
| $h_{down}$ | $\infty$ |
| $d_0$ | 30-1500 $\mu$m |
| $f$ | 193.5 THz |
| $n_{down}$ | 3.47 (Silicon, metal otherwise) |
| $n_{slb}$ | 1.44 (Silica) |
| $n_{up}$ | 1 (Air) |
| antenna Gain | 15-25 dB |

## IV. System Modeling and Performance Evaluation

The performance of a communication link is usually characterized in terms of BEP, or measured as bit error rate from an experimental setting. For the design of networks with wireless links, it is very important to adopt an interference-aware framework for BEP evaluation, exploiting the analysis carried out in [18]. Cross-link interference may occur among simultaneously transmitting links that use the same optical channel, as illustrated in Section II. Within this framework, a network designer can find the optimal link configurations that meet the required performance for on-chip communication. For the performance analysis, we assume that all links use intensity modulation On-Off Keying (OOK) with Non-Return-to-Zero (NRZ) pulses and direct detection. If the bits of the data sources have the same probability 1/2, the average power of the modulated signal is one half of the power of the unmodulated carrier, also named here as optical power. The optical power of the received desired signal is denoted by $P_0$, and the optical power of the $i$-th received interfering signal, normalized to the desired optical power, is denoted by $x_i = P_i/P_0$, with $i = 1, 2, ..., N$. The received powers are functions of the geometry of the links, the distances and the angles between the antennas, the antenna design, the propagation characteristics of each link. For a given transmitted optical power, $P_T$, the received power is given by $P_i = GP_iP_T$ , where $GP_i$ is the path gain of the channel between transmitter $i$ and reference receiver, which is obtained with the RT tools, as shown in Section III.

The BEP is one of the principal metrics that allows to describe the overall communication performance, which is evaluated as the function of Signal-to-Noise Ratio (SNR) and interference powers ($x_i$'s). In the analysis, SNR $= 4\,\gamma^2$, $\gamma = \eta_{\text{PD}} P_0/(2\sigma_{\text{th}})$ depends on the unmodulated received power, $\eta_{\text{PD}}$ is the responsivity of photodetector, and $\sigma_{th}$ is the standard deviation of the additive Gaussian noise at the receiver. The dominant noise at the *p-i-n* receivers usually is the thermal noise [19]. Therefore, noise variance $\sigma_{th}^2$ does not depend on transmitted bits and is given by $\sigma_{th}^2 = 4KT_{eq}/(2R_LT)$, where $K$ is the Boltzman's constant, $T_{eq}$ is the noise temperature of the receiver, $R_L$ is the resistance of the receiver and $T = 1/R_b$ is the bit interval of data transmission with $R_b$ the data-rate of the links. Recall that the probability of detecting the photocurrent transmitting *zero* above the decision threshold, or detecting the photocurrent transmitting *one* below the threshold at the receiver is evaluated as the BEP. In particular, the BEP is given by $\overline{P}_{\text{b}}(\gamma, x_1, ..., x_I) = \mathbb{E}\{P_{\text{b}|b_i,\phi_i,\tau_i}(\gamma, x_1, ..., x_N)\}$ through the analytical method in [18], where $\mathbb{E}\{.\}$ is the expected value taken over the Random Variables (RVs) in the optical wireless communication system. The RVs include the transmitted bits $b_i$ with one-half probability of being one or zero, the phases $\phi_i$ of the optical carriers at the receiver and the time offsets $\tau_i$ of the asynchronous interfering links, which are uniformly distributed on $[0, 2\pi]$ and $[0, T]$, respectively, for $i = 1, ...N$.

## V. Numerical Results

We examine some link scenarios by using the experimental measurements from RT. The principal parameters are given in Table I. In the results, the chip is assumed to be sufficiently large, such that the reflected rays from the lateral sides in the $xy$ plane can be neglected. For example, consider a distance of

 ISBN: 978-1-61208-749-8 

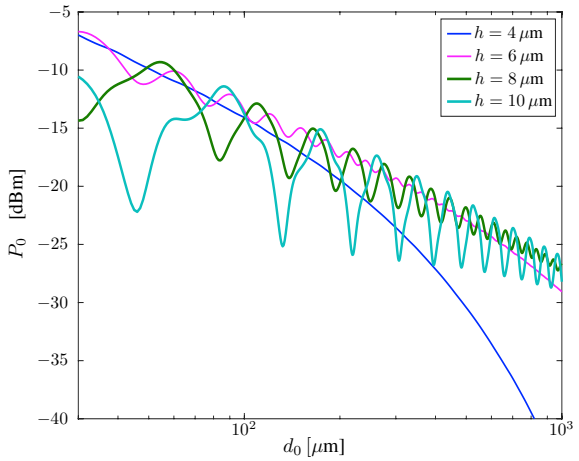


Figure 4. Received power vs distance $d_0$ with $G = 20$ dB and different values of $h_{\text{slb}}$ [$\mu$m] without interfering link

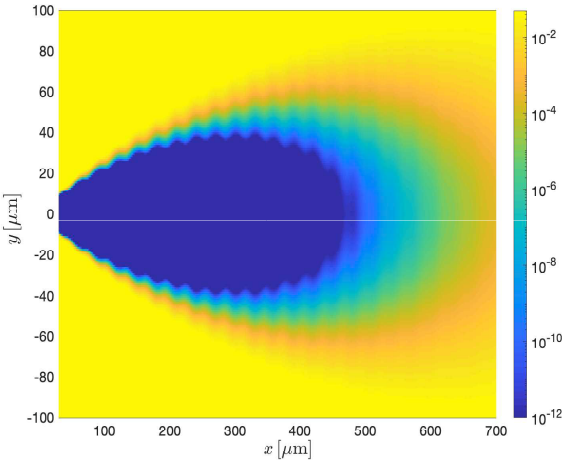


Figure 6. BEP vs position of $\text{RX}_0$ antenna in the $xy$ plane with $G = 20$ dB, $h_{\text{slb}} = 6\,\mu$m, and without interfering link.

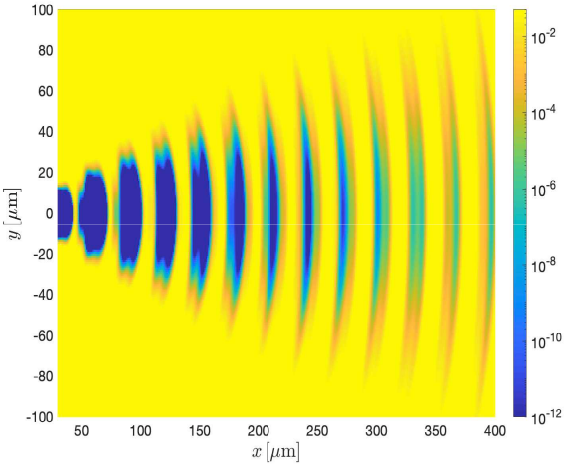


Figure 5. BEP vs position of $\text{RX}_0$ antenna in the $xy$ plane with $G = 15$ dB, $h_{\text{slb}} = 6\,\mu$m, and without interfering link.

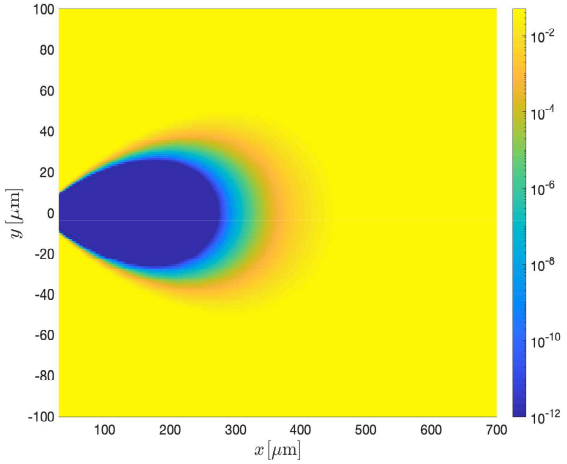


Figure 7. BEP vs position of $\text{RX}_0$ antenna in the $xy$ plane with $G = 20$ dB, $h_{\text{slb}} = 4\,\mu$m, and without interfering link.

at least 500 $\mu$m from transmit/receive antennas to the lateral sides of the chip. Therefore, only the reflections from the interfaces between the $SiO_2$ slab, and upper and lower layers ($xz$ plane) contribute to the aggregate received signal. The $\text{TX}_0$ is located at the origin of the 3D coordinate system ($x_{\text{TX}_0} = y_{\text{TX}_0} = z_{\text{TX}_0} = 0$), where $z = 0$ at the middle of the $SiO_2$ slab and for all transmitters and receivers $z = 0$. For all results, the average power of all the transmitted signals is 0 dBm, the data-rate is $R_b = 10$ Gbit/s and the parameters of the receiver are $\eta_{\text{PD}} = 0.7$ A/W, $T_{eq} = 600$ K, $R_L = 1000\,\Omega$. Figure 4 shows the received power $P_0$ in dBm vs the distance of $d_0$ $\mu$m for the wireless link as shown in Figure 1, when the antennas of $\text{TX}_0$ and $\text{RX}_0$ are aligned, i.e., $\theta_{\text{T}_{0,0}} = \theta_{\text{T}_{0,0}} = 0$. The results are provided for the antennas with $G = 20$ dB and different values of the slab layer thickness ($h_{\text{slb}}$). It is shown that by increasing the thickness, the fluctuations of the results increase and at large distances, the power level decays slowly with higher thickness compared to the cases with smaller thickness.

Figures 5 to 7 map the BEP over the positions of the antenna of receiver $\text{RX}_0$ in a two dimensional $xy$ plane, when the antenna of the desired transmitter $\text{TX}_0$ is located at the origin $(x = 0, y = 0)$ and the interfering link is absent. The values of the BEP are shown by colorbars. The antenna gain is $G = 15$ dB with $h_{\text{slb}} = 6$ $\mu$m in Figure 5, whereas $G = 20$ dB, and $h_{\text{slb}} = 4$ $\mu$m and 6 $\mu$m are considered in Figures 7 and 6, respectively. The area with $P_{\text{b}} \leq 10^{-8}$ can be considered as a *coverage* domain for the given setting (blue domain). As shown, the *coverage* domain in Figure 5 is not regular, which is due to received power fluctuations resulting from multipath propagation. The domain is composed of a number of separated zones and the maximum coverage distance achievable without interruptions is limited to 40 $\mu$m. By increasing the antenna gain the *coverage* domain

 ISBN: 978-1-61208-749-8 

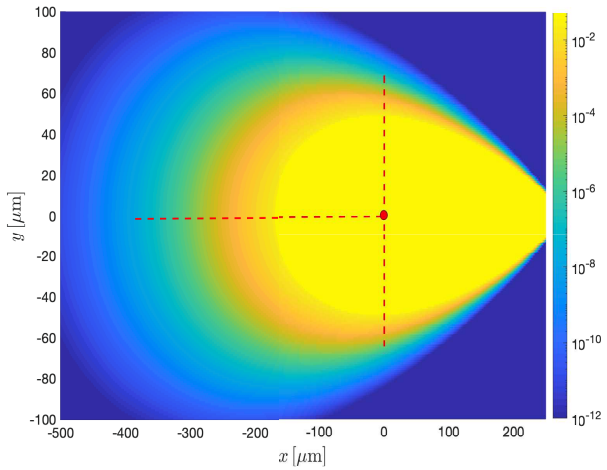


Figure 8. BEP vs position of $\mathrm{TX}_1$ antenna in the $xy$ plane with $G = 20$ dB, $h_{\mathrm{slb}} = 4\,\mu$m, where $d_0 = 280\,\mu$m.

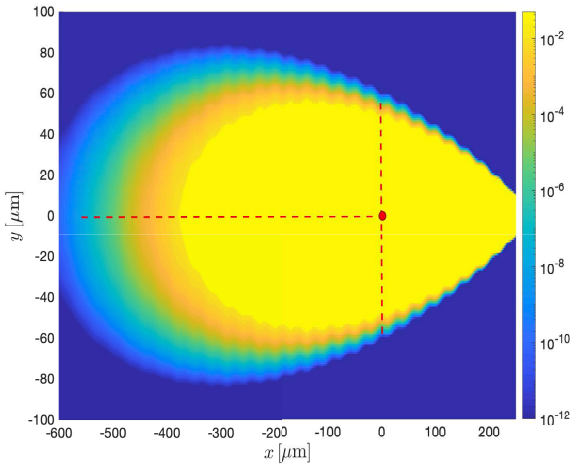


Figure 9. BEP vs position of $\mathrm{TX}_1$ antenna in the $xy$ plane with $G = 20$ dB, $h_{\mathrm{slb}} = 6\,\mu$m, where $d_0 = 280\,\mu$m.

becomes larger and continuous, as shown in Figures 6 and 7. In fact, by reducing the antenna beamwidth, also the multipath induced power fluctuations become small. The coverage is guaranteed for a maximum distance of roughly $480$ $\mu$m in Figure 6. Received power fluctuations can be further reduced by decreasing the slab thickness, as shown in Fig 7 for $h_{\mathrm{slb}} = 4$ $\mu$m. However, the coverage distance decreases to roughly $280$ $\mu$m for $h_{\mathrm{slb}} = 4$ $\mu$m. This happens because, with few multipath components the received power decreases more rapidly at large distances, as seen in Figure 4.

In Figures 9, 10 and 11, the BEP values are mapped over the positions of an interfering transmitter $\mathrm{TX}_1$ in two dimensional $xy$ plane, where the antennas of $\mathrm{TX}_0$ and $\mathrm{RX}_0$ are aligned and the distance $d_0$ is fixed to a given value. Note that $d_0$ is selected inside the *coverage* domain, as mentioned for example in Figure 7 and Figure 6.

Figure 8 and Figure 9 examine $h_{\mathrm{slb}} = 4$ and $6$ $\mu$m, respectively, to provide a comparison between different values of the slab thickness, considering $G = 20$ dB and $d_0 = 280$ $\mu$m (inside the *coverage* area for both cases). The red point at the origin ($x = 0$, $y = 0$) shows the desired transmitter position. Here, we denote the domain with $P_{\mathrm{b}} \geq 10^{-8}$ (green-yellow domain) as *not allowed* domain for an adjacent transmitter that interfere with the desired link. It can be observed that the case with $h = 6$ $\mu$m experiences more fluctuations in the BEP values since both the useful and interfering signals are subject to more fading with respect to the case with $h_{\mathrm{slb}} = 4$ $\mu$m. Consider an interfering link parallel to the desired one, i.e., $x = 0$, $y \neq 0$ for the adjacent transmitter. In order to maintain $P_{\mathrm{b}} \leq 10^{-8}$, the adjacent transmitter cannot be placed on the vertical dashed line, thus $\Delta = |y| \geq 74$ $\mu$m. By increasing $h_{\mathrm{slb}}$ in Figure 9, $\Delta$ decreases to $45$ $\mu$m, therefore, for parallel links increasing the thickness can reduce the reuse distance. Consider an interfering link aligned to the desired one, ($x \neq 0$, $y = 0$) with a transmitter that has the same

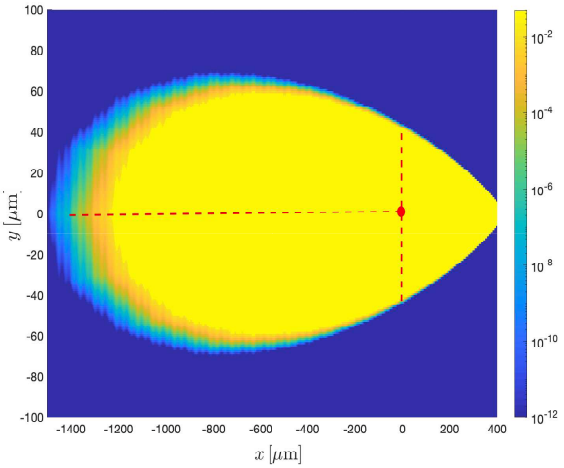


Figure 10. BEP vs position of $\mathrm{TX}_1$ antenna in the $xy$ plane with $G = 25$ dB, $h_{\mathrm{slb}} = 6\,\mu$m, where $d_0 = 430\,\mu$m.

antenna axis direction as the desired transmitter. The horizontal dashed line shows the not allowed positions for the interfering transmitter. For the case of $h_{\mathrm{slb}} = 4$ $\mu$m, the distance between two transmitters must be greater than $380$ $\mu$m (the horizontal line length), while for the case with $h_{\mathrm{slb}} = 6$ $\mu$m this distance increases to $430$ $\mu$m. It can be described by the fact that the multipath component decreases for smaller $h$, therefore the interference power decays more rapidly for the case with $h_{\mathrm{slb}} = 4$ $\mu$m, as seen in Figure 4.

In Figure 10, $G = 25$ dB, $h_{\mathrm{slb}} = 6$ and $d_0 = 430$ $\mu$m are considered. In such case, despite the high value of $d_0$ compared to Figure 9, $P_{\mathrm{b}} \leq 10^{-8}$ can be satisfied with $\Delta \geq 43$ $\mu$m to positioning the adjacent transmitter for a parallel wireless link. It can be observed that, the distance between two horizontally aligned transmitters is increased to $1.470$ mm. In fact, by increasing the antenna gain to $25$ dB, the received

 ISBN: 978-1-61208-749-8 

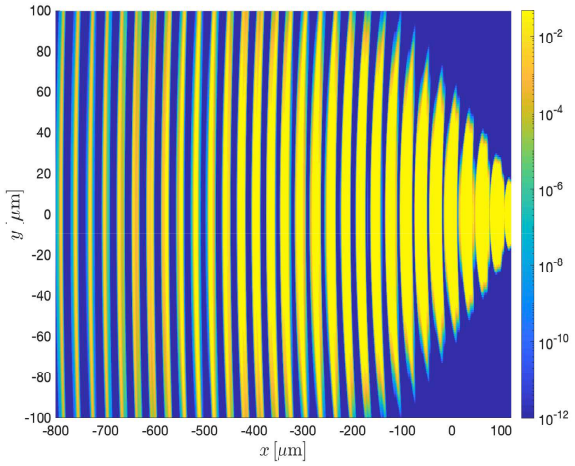


Figure 11. BEP vs position of $TX_1$ in the $xy$ plane with $G = 15$ dB, $h_{\text{slb}} = 6\,\mu$m, where $d_0 = 150\,\mu$m.

power by an interfering transmitter that is aligned horizontally to the desired transmitter decays significantly only at a large distance.

In Figure 11, $G = 25$ dB and $h_{\text{slb}} = 6$ with $d_0 = 430\ \mu$m are considered. In such case, the optical system is subject to high fading, as shown in Figure 5 for the same $G$ and $h_{\text{slb}}$ without interference. Therefore, the results vs the positions of $TX_1$ show a marked non regularity for *not allowed* domain, as well as for *coverage* domain in Figure 5.

## VI. Conclusions

Optical wireless (OW) links as components of a network-on-chip (NoC) have been analyzed in the presence of multipath propagation, co-channel interference and noise. The wireless channel has been characterized by using a RT method applied to the on-chip scenario. The communication performance in terms of the BEP has been evaluated accounting for the statistics of random variables in the OW communication system. The effect of antenna directivity, geometrical parameters of the chip structure and wireless links, and the number of interfering links on the BEP have been investigated. Different link configurations have been examined, and the BEP has been plotted on grid maps with $1\,\mu$m accuracy. The analysis helps determine supportable domains for the position of the link components, i.e., transmit and receive antennas, such that the required BEP is guaranteed. It has been shown that, for antennas with low directivity, the fading in OW channels can cause discontinuity in a supported domain. The fading is also subject to the thickness of the $SiO_2$ slab layer. Therefore, finding the optimal thickness for this layer can improve considerably the on-chip communication link performance.

## Acknowledgment

Research activity has been supported by PRIN 2015 Project "Wireless Networks through on-chip Optical Technology (WiNoT)".

## References

[1] M. Nafari, L. Feng, and J. Jornet, "On-chip wireless optical channel modeling for massive multi-core computing architectures," in *Proc. IEEE Wireless Commun. and Networking Conf.*, San Francisco, CA, USA, Mar. 2017, pp. 1–6.

[2] G. Bellanca, G. Calo, A. E. Kaplan, P. Bassi, and V. Petruzzelli, "Integrated Vivaldi plasmonic antenna for wireless on-chip optical communications," *Optics Express*, vol. 25, no. 14, pp. 16 214–16 227, Jun. 2017.

[3] L. Benini and G. D. Micheli, "Networks on chips: a new SoC paradigm," *IEEE Computer*, vol. 35, no. 1, pp. 70–78, Jan. 2002.

[4] J. D. Owens et al., "Research challenges for on-chip interconnection networks," *IEEE Micro*, vol. 27, no. 5, pp. 96–108, Nov. 2007.

[5] J. Kim, K. Choi, and G. Loh, "Exploiting new interconnect technologies in on-chip communication," *IEEE J. Emerg. Select. Top. Circuits Syst.*, vol. 2, no. 2, pp. 124–136, Jun. 2012.

[6] A. Biberman and K. Bergman, "Optical interconnection networks for high-performance computing systems," *Reports on Progress in Physics*, vol. 75, no. 4, pp. 046 402–046 416, Apr. 2012.

[7] S. Werner, J. Navaridas, and M. Luján, "A survey on optical network-on-chip architectures," *ACM Comput. Surv.*, vol. 50, no. 6, pp. 89:1–89:37, Dec. 2017.

[8] M. A. I. Sikder, A. K. Kodi, M. Kennedy, S. Kaya, and A. Louri, "OWN: Optical and wireless network-on-chip for kilo-core architectures," in *IEEE 23rd Annu. Symp. High-Perform. Interconnects*, Santa Clara, CA, USA, Aug. 2015, pp. 44–51.

[9] D. DiTomaso et al., "A-WiNoC: Adaptive wireless network-on-chip architecture for chip multiprocessors," *IEEE Trans. Parallel Distrib. Syst.*, vol. 26, no. 12, pp. 3289–3302, Dec. 2015.

[10] M. O. Agyeman et al., "A resilient 2-D waveguide communication fabric for hybrid wired-wireless NoC design," *IEEE Trans. Parallel Distrib. Syst.*, vol. 28, no. 2, pp. 359–373, Feb. 2017.

[11] S. Abadal, A. Mestres, J. Torrellas, E. Alarcon, and A. Cabellos-Aparicio, "Medium access control in wireless network-on-chip: A context analysis," *IEEE Commun. Mag.*, vol. 56, no. 6, pp. 172–178, Jun. 2018.

[12] S. Abadal, A. Mestres, M. Nemirovsky, H. Lee, A. Gonzàlez, E. Alarcòn, and A. Cabellos-Aparicio, "Scalability of broadcast performance in wireless network-on-chip," *IEEE Trans. Parallel Distrib. Syst.*, vol. 27, no. 12, pp. 3631–3645, Dec. 2016.

[13] J.-J. Lin, L. Gao, A. Sugavanam, X. Guo, R. Li, J. E. Brewer, and K. K. O, "Integrated antennas on silicon substrates for communication over free space," *IEEE Electron Device Lett.*, vol. 25, no. 4, pp. 196–198, Apr. 2004.

[14] H. K. Mondal, S. H. Gade, M. S. Shamim, S. Deb, and A. Ganguly, "Interference-aware wireless network-on-chip architecture using directional antennas," *IEEE Trans. Multi-Scale Comput. Syst.*, vol. 3, no. 3, pp. 193–205, Jul. 2017.

[15] F. Fuschini, M. Barbiroli, M. Zoli, G. Bellanca, G. Calò, P. Bassi, and V. Petruzzelli, "Ray tracing modeling of electromagnetic propagation for on-chip wireless optical communications," *J. Low Power Electron. Appl.*, vol. 8, no. 4, pp. 39–54, Oct. 2018.

[16] D. Matolak, S. K. A. Kodi, D. D. Tomaso, and W. R. S. Laha, "Wireless networks-on-chips: architecture, wireless channel, and devices," *IEEE Wirel. Commun.*, vol. 19, no. 5, pp. 58–65, 2012.

[17] D. Vantrease et al., "Corona: System implications of emerging nanophotonic technology," in *Int. Symposium on Computer Architecture*, Beijing, China, Jun. 2008, pp. 153–164.

[18] J. Shafiei Dehkordi and V. Tralli, "Interference analysis for optical wireless interconnections," in *Proc. IEEE Int. Symp. on Personal, Indoor and Mobile Radio Commun.*, Bologna, Italy, Sep. 2018, pp. 1–7.

[19] G. P. Agrawal, *Lightwave Technology: Telecommunication Systems*. Hoboken, NJ: Published by John Wiley & Sons, Inc., 2005.

 ISBN: 978-1-61208-749-8 